

Picosecond shear waves in nano-sized solids and liquids

T. Pezeril^{a,b}, C. Klieber^b, S. Andrieu^c, D. Chateigner^d and K. A. Nelson^b

^aLPEC, UMR CNRS 6087, Université du Maine, 72000 Le Mans, France;

^bDepartment of Chemistry, Massachusetts Institute of Technology, 02139 Cambridge, USA;

^cLPM, UMR CNRS 7556, Université H. Poincaré, 54506 Vandoeuvre, France;

^dCrismat-Ensicaen, UMR CNRS 6508, Université de Caen Basse-Normandie, 14050 Caen, France.

ABSTRACT

We will review recent progress on the generation and detection of picosecond shear acoustic waves. Examples will be shown in which the transverse isotropic symmetry of the sample structure is broken in order to permit shear wave generation through sudden laser heating. As an illustration of the technique, picosecond longitudinal and shear acoustic waves have been successfully employed to probe structural dynamics in nano-sized solids (gold nano-crystals assemblies) and nano-sized liquids (glycerol and water).

Keywords: Picosecond ultrasonics

1. INTRODUCTION

The development of picosecond ultrasonics,¹⁻³ in which single-cycle acoustic wavepackets are generated through sudden laser heating of a thin film and detected optically after propagation through one or more film and/or substrate layers, has been exploited for thin film diagnostics and for measurement of acoustic properties in the ~ 50 -500 GHz frequency and ~ 10 -100 nm wavelength ranges. The method has been applied to a wide range of materials, but in general it has been restricted to generation and characterization of longitudinal acoustic waves.⁴ High-frequency, short-wavelength shear acoustic properties would be of great interest in many materials, especially disordered and partially ordered systems such as supercooled liquids and glasses, mixed ferroelectrics and multiferroics, and giant magnetoresistance or other correlated electron systems in which fast relaxation dynamics or mesoscopic correlation lengths of quantities that are coupled to shear play important roles. Recently, examples have emerged in which the transverse isotropic symmetry of the sample structure is broken in order to permit shear wave generation through sudden laser heating. Thus, shear acoustic wave components were generated in an off-axis oriented Zn single crystal,⁴⁻⁷ see Figure 1, or by use of an off-axis TeO₂ transparent substrate coated by an Al layer.⁸ These examples illustrated different possibilities for shear wave generation, but their requirements for specialized material fabrication or acoustic wave generation conditions reduce their versatility for use with a wide range of materials, specially liquids where the shear damping is the strongest.

In the following sections, we describe how recently developed samples are employed for the generation of picosecond shear waves, and demonstrate their feasibility to perform measurements in liquids. The first section shows examples where shear waves have been experimentally identified in gold films constituted of canted nano-crystals through the observation of acoustic resonance of the entire structure.⁹ The second section demonstrates the potential of this type of photoacoustic shear transducer for the investigation of relaxation dynamics in liquids. We will describe a novel technique dedicated to the measurement of shear relaxation dynamics in liquids that yielded results of shear viscoelastic properties in glycerol and water at gigahertz frequencies.

Further author information: (Send correspondence to thomas.pezeril@univ-lemans.fr)

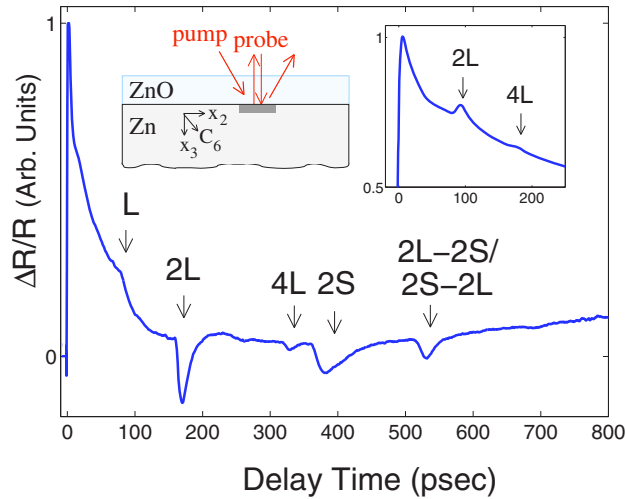


Figure 1. Change in transient reflectivity of a Zn single-crystal substrate with tilted C_6 axis relative to the interface normal on which a transparent ZnO film has been deposited. The break of shear symmetry allows for the direct thermoelastic generation of plane shear waves which are partially transmitted into the ZnO film. After a round trip inside the ZnO film, the shear acoustic wavepacket is detected (see the 2S echo in the transient reflectivity signal). The excitation of longitudinal waves does not require such a canted symmetry. Thus, in the case of a Zn single crystal whose normal surface coincides with the C_6 axis, see inset top right, only longitudinal waves are excited (as revealed by the detection of the 2L and 4L longitudinal echoes in the transient reflectivity signal only).

2. CANTED GOLD NANOCRYSTALS ASSEMBLIES ON SILICON

In the present section, we demonstrate the possibility of shear wave generation and detection in an extremely simple system: a thin gold film constituted of nanocrystals on a silicon single crystal substrate. We describe experimental observation of a fundamental shear mode of vibration, in addition to the fundamental longitudinal mode observed ordinarily.^{1-3, 10-15}

The samples are thin gold films of different thicknesses deposited on silicon (100) single crystals by DC sputtering. The thicknesses of the films were measured using x-ray reflectivity,¹⁶ with an accuracy of ~ 0.1 nm. For the picosecond photoacoustic experiments we used a conventional pump-probe technique with a Ti:sapphire laser operating at 800 nm. The output is split into a pump and a variably delayed probe beam that are focused and crossed at the sample. Each pump pulse induces a thermal stress in the absorptive gold film which is responsible for photoacoustic excitation. The time-dependant probe reflectivity is sensitive to the acoustic perturbation of the dielectric coefficient $\delta\epsilon$, proportional to the strain. Results of reflectivity changes ΔR for the sample of 8.3 nm thickness are presented in Fig. 2. The two modes of vibration that we assume to be of mainly longitudinal (L) and shear (S) acoustic character are clearly visible for a 800 nm probe wavelength. In case of probing with a probe wavelength of 400 nm instead of 800 nm, the shear wave is undetected in this case. This drastic difference suggests that the dispersion of the photoelastic coefficients p_{ij} with the probe wavelength results in a strong reduction at 400 nm in the magnitude of the combination $p_{44} - \frac{p_{11} - p_{12}}{2}$ (on which shear detection depends) while the magnitude of the coefficient p_{12} (which determines the detection sensitivity for longitudinal strains) is comparable at 400 nm and 800 nm probe wavelengths.

X-ray combined analysis¹⁷ was used to quantitatively determine the crystallographic textures, mean crystallite sizes and cell parameters of the gold films. X-ray analysis revealed that on average the individual crystallites occupy the whole thickness of the films and that the orientations of 60% of the crystallites are different from the high symmetry texture $\langle 111 \rangle$ orientation. In other words, these DC sputtered gold structures can be seen as the transposition at the nanometric scale of the results obtained earlier for zinc samples,^{4, 7, 18} and the same theoretical argument for shear generation and detection holds for this scenario. Simulations of photoacoustic wave generation in gold single crystals have shown substantial quasishear amplitude for a broad range of orientations¹⁹

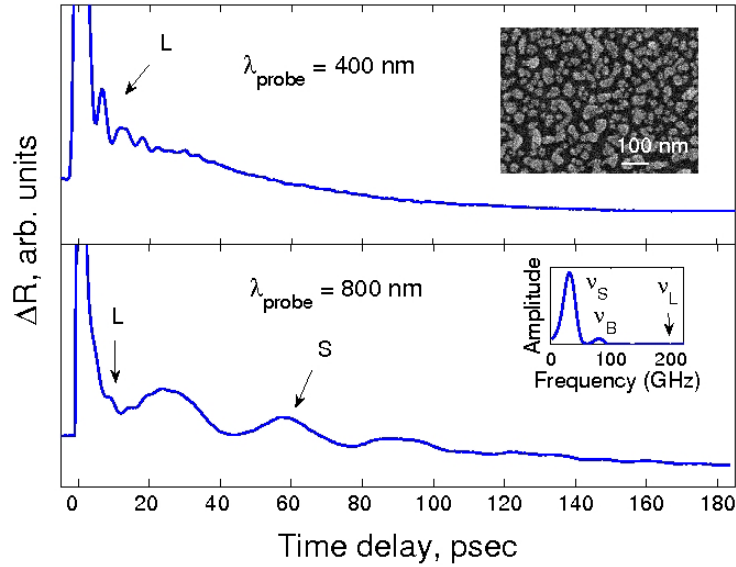


Figure 2. Probes at 800 nm and 400 nm detect dynamic reflectivity changes ΔR from the sputtered gold film nanostructure (inset, top right). It should be noted that for thicker films, the gold nanocrystals are clearly in contact. Shear waves S are only detected at 800 nm, while longitudinal waves L are visible at both probe wavelengths. The inset shows the Fourier transform with their ringing frequencies ν_S , ν_L . The frequency ν_B is due to the longitudinal Brillouin backscattering in the silicon substrate.

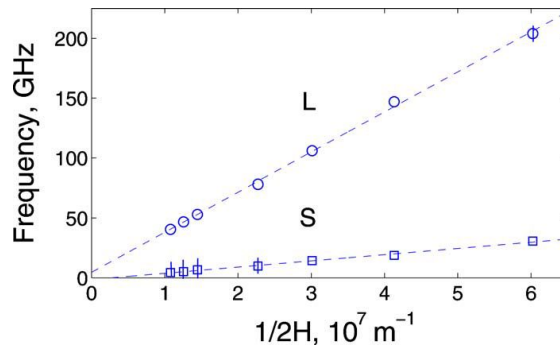


Figure 3. Dispersion curves of both longitudinal and shear modes of the gold films. The slopes give the average acoustic speeds in the films. The intercepts are zero within experimental uncertainties.

and thus, many of the nanocrystallite orientations are expected to have significant shear generation efficiency. For the detection, it is the deviation from isotropy in the photoelastic interaction that allows the detection of the shear waves. For any cubic medium, the change in dielectric coefficient $\delta\epsilon_s$ from shear strain η_s is given by $\delta\epsilon_s = \epsilon^2 \sin 2\chi \cos 2\chi (p_{44} - \frac{p_{11}-p_{12}}{2}) \eta_s$,¹⁸ where χ is the angle between the sample normal and the $\langle 111 \rangle$ crystallographic direction. Since $p_{44} \neq \frac{p_{11}-p_{12}}{2}$ and χ is statistically nonzero in more than 60% of the films, the detection of shear acoustic waves is qualitatively justified as well. It should be also noted that in gold films of $\langle 111 \rangle$ texture, as for RF sputtered gold samples studied by other groups,¹⁴ no frequency except the longitudinal L frequency has been observed.

The longitudinal and shear resonance frequencies ν_L and ν_S respectively for all the film thicknesses have been extracted through Fourier analysis of the reflectivity signals and plotted versus $1/2H$ as shown in Fig. 3. The longitudinal frequencies follow the linear dispersion relation, $\nu_L = c_L/2H$, where $c_L = 3340 \text{ ms}^{-1}$ is the mean

longitudinal acoustic velocity deduced from the slope of the L mode of the dispersion curve of Fig. 3. This dispersion behavior is expected since the acoustic impedance $Z_L^{Au}/Z_L^{Si} \sim 3.3 > 1$. The shear mode frequencies follow the dispersion relation, $\nu_S = c_S/4H$, where $c_S = 1040 \text{ ms}^{-1}$ is the mean shear acoustic velocity. This value is in close agreement with the expected shear speed of sound that corresponds to the broad maximum of the simulated quasishear photoacoustic excitation. This dispersion behavior is expected if $Z_S^{Au}/Z_S^{Si} < 1$. The values that we determine for c_S and the gold film density (from the x-ray data) as well as the same parameters for Si would yield the opposite result, i.e. $Z_S^{Au}/Z_S^{Si} \sim 1.6 > 1$. We believe this shear dispersion discrepancy could be a signature of poor contact of gold to silicon.

These results have shown new possibilities for generation and detection of ultrahigh-frequency shear waves in gold films deposited through routine DC sputtering. A next step would be the exploration of different deposition conditions and techniques and different materials to determine the extent of possible control over the asymmetric structure of the layers and the ranges of shear acoustic wave parameters that might be reached. In the following section we employed a semi-transparent iron thin film grown through MBE, under specific conditions of deposition with full control of the canted symmetry,²⁰ which allowed us the study of shear waves in liquids.

3. PICOSECOND SHEAR WAVES IN LIQUIDS

Fast structural relaxation dynamics in liquids continue to pose major fundamental challenges,²¹ in large measure because direct experimental access to key relaxing degrees of freedom over the time or frequency ranges of interest remains elusive. Both density and shear relaxation play central roles in the complex structural responses of viscoelastic materials. Fast responses require measurements of shear acoustic waves in the megahertz and gigahertz frequency ranges. Much of the MHz range is now accessible to ultrasonics and impulsive stimulated thermal or Brillouin scattering (ISTS or ISBS respectively^{22–26}). Picosecond ultrasonics has provided tabletop access to much of the GHz frequency range for longitudinal acoustic waves and the adaptation of this method to GHz shear wave generation is in progress. However, probing shear waves in liquids have remained elusive, to the extent that the challenges in "Seeking shear waves in liquids with picoseconds ultrasonics"²⁷ have been elaborated explicitly.

In this section we describe an approach for generating frequency-tunable shear as well as longitudinal acoustic waves in the GHz frequency range. We further demonstrate a sample and optical configuration that allows to conduct measurements in viscoelastic liquids, whose GHz-frequency acoustic responses are of particular interest in the context of the study of complex structural relaxation dynamics. We present results from glycerol and water at room temperature, where shear acoustic waves up to 50 GHz were characterized. Our approach opens the door to versatile shear and longitudinal acoustic spectroscopy of bulk materials and of nanometer solid and liquid layers down to monolayer thicknesses.

In the present front-back optical pump-probe type measurement, see Figure 4(A), longitudinal and shear acoustic waves were optically generated in an iron semi-transparent thin film upon ultrafast laser irradiation. The iron films of about 50 nm thickness were obliquely deposited under ultra-high vacuum,²⁰ with an oblique incidence angle of 60° , providing a tilt of the crystal symmetry axis of about 40° , see Fig 4(B). The canted symmetry of the iron film ensures direct generation of shear acoustic wave. Both, longitudinal and shear acoustic waves may propagate into an adjacent layer of liquid, and be detected directly in a transparent propagating medium through time-domain Brillouin light scattering, as soon as they have crossed the liquid film. The strain pulses interacts with the liquid which leads to spatial broadening and distortion due to frequency-dependent damping and dispersion. In the transparent substrate medium, the broadened propagating longitudinal and shear strains perturb the permittivity tensor which back-scatters and depolarizes (only in the shear case) the incoming probe light. This effect is known as coherent (depolarized in the shear case) Brillouin scattering. In the present configuration, this phenomenon was observed in the time domain as an oscillatory signal at the so-called Brillouin frequency, see Fig. 4(C). This frequency ν is determined by the probe wavelength λ , the angle of incidence θ , and the refractive index n and acoustic speed v in the propagating medium through the formula $f = (2nv/\lambda) \cos(\theta)$. Longitudinal and shear acoustic wave packets travel at different speeds resulting in two different tandem Brillouin frequencies. The peculiar interaction of propagating shear waves with light entails the back-scattered light portion to be depolarized and hence allows for their detection through depolarized Brillouin scattering at oblique incidence.⁶ Typically, the signal to noise levels of the recorded signals are rather

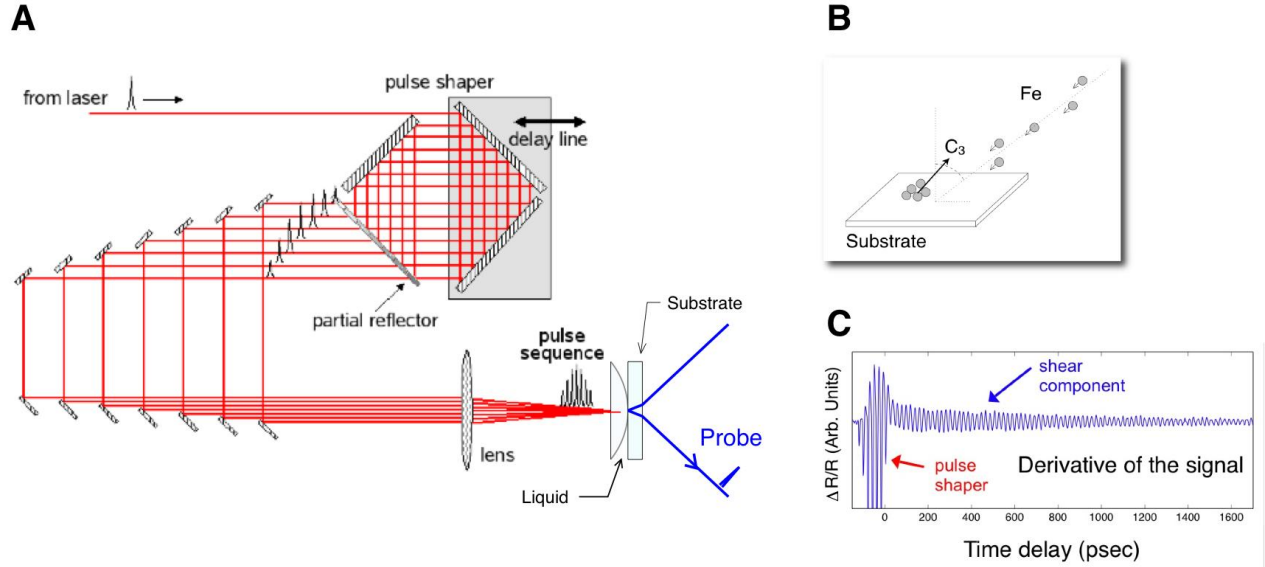


Figure 4. (A) Schematic illustration of the optical pulse shaper at 800 nm laser wavelength. The sample cell is made of a liquid which is squeezed between a transparent flat substrate and a plano-convex lens. The curved side of the lens is coated with an iron thin film with canted crystallographic orientation and a sequence of seven optical excitation pulses generates multiple-cycle acoustic waves in the iron film. After propagation through the liquid layer, the acoustic waves are detected in the transparent solid substrate by time-resolved coherent Brillouin scattering of variably delayed 400 nm probe pulses. (B) The iron films were deposited through MBE at oblique incidence. (C) The pulse sequence timing is adjusted to match either the longitudinal or shear Brillouin frequency of the substrate, to enhance their respective spectral brightness.

poor and our approach to overcome this shortcoming is the excitation of narrowband (multiple-cycle) acoustic wave packets. This is accomplished by generating a pulse sequence with tunable frequency²⁸ and thus resonantly enhance the extremely weak shear Brillouin scattering frequency components. Combining these two techniques allows us to quantitatively analyze the interaction of high-frequency shear waves with liquids. Unlike usual Brillouin spectroscopy, this experimental approach enable the measurement not only of the amplitude but also of the phase of the Brillouin scattering that is linked to the acoustic information of the liquid medium.

The detected probe light undergoes time-dependent intensity modulation δI ,

$$\delta I = A \cos(2\pi\nu t + \phi), \quad (1)$$

where,

$$A \propto \exp(-\Gamma d), \quad \phi \propto -2\pi\nu(d/v), \quad (2)$$

at the Brillouin frequency ν of the gauge material. Here, the Brillouin phase shift ϕ is proportional to the traveling time of the acoustic wave through the liquid of thickness d at the acoustic speed v . The Brillouin scattering amplitude A is given by the liquid sample thickness and the attenuation coefficient Γ . In our analysis, we have also taken into account the modification of the optical phase due to the variation in liquid thickness in throughout a series of experiments, but it turns out that the acoustic phase shift ϕ of equation (2) is predominant and accurately describes our experimental situation. The analysis of the overall phase shift allows for a precise thickness determination down to a couple of nanometer. For example, at a longitudinal Brillouin frequency of 90 GHz in sapphire and a longitudinal speed of sound of about 3000 m/s in glycerol, a full cycle phase shift corresponds to only 33 nm liquid thickness, and a molecule of 0.5 nm in diameter will create a phase shift of 5.5° which is easily measurable.

Our experimental approach for the determination of high-frequency longitudinal and shear acoustic properties of liquid glycerol comprises of a sequence of steps. We start by recording the time resolved longitudinal Brillouin

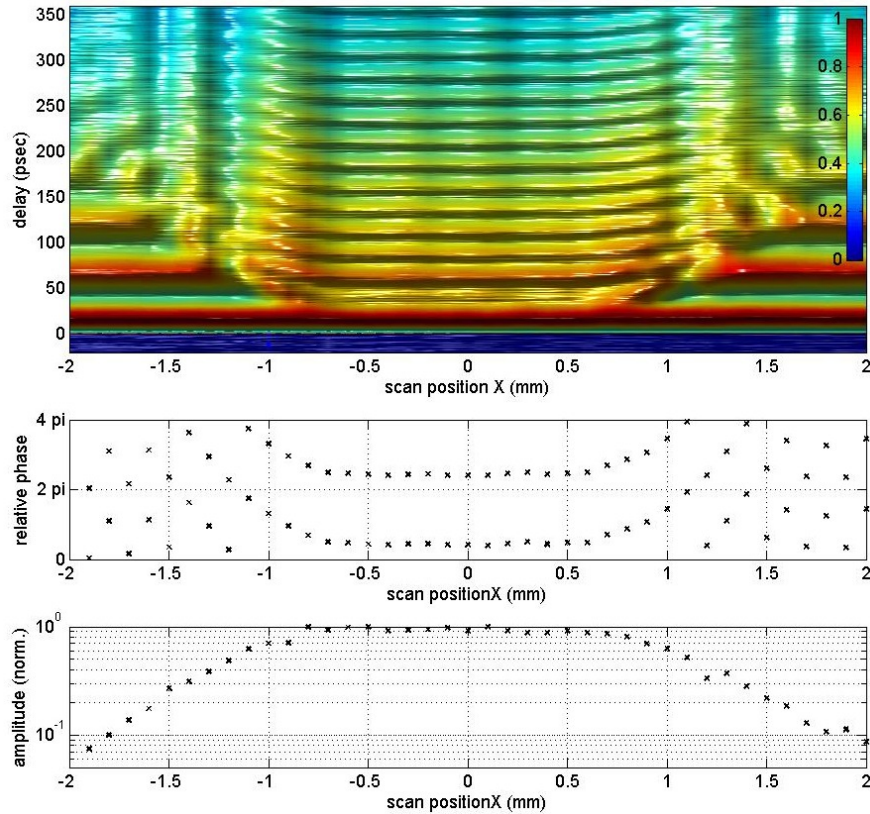


Figure 5. (Top figure) Interpolated 2D plot of about 40 longitudinal wave data sets recorded as a function of probe delay time (plotted vertically) at different lateral (X) positions across the sample (displayed horizontally). A single excitation pulse rather than a pulse sequence was used in this case. The high-frequency signal oscillations at 40 GHz correspond to Brillouin scattering from longitudinal acoustic waves in the BK7 glass substrate while the low-frequency oscillations at 18 GHz correspond to Brillouin scattering from the acoustic waves in liquid glycerol. Away from the center of the sample ($|X| > 0.5$ mm) the transit time through the liquid layer is apparent as a delay in the start of substrate acoustic propagation and a phase shift in the signal oscillations relative to the phase at the center of the sample. Normalized amplitude values and phase shifts of the 40 GHz high-frequency Brillouin signal oscillations from the spectrum analysis of the signal displayed in the top figure.

scattering at different X positions on the lens as shown in Figure 5. Next, according to formula (2) and the known curvature of the lens that allows the determination of the liquid thickness topography, the Fourier analysis of the Brillouin signal yielded the value of the mean longitudinal speed of sound and attenuation over the whole scanned area. The contribution of the optical cavity effect to the overall amplitude of the back-scattered light was eliminated by normalizing the amplitudes in each scan series with the laser pump trace as a reference. The acoustic cavity effect of the confined liquid which could modulate the overall acoustic amplitude has been neglected, mainly because it does not appear in the raw amplitude measurements. Both of these artifacts, whether due to the acoustic or optical cavity effect, could dramatically alter the results of the speed of sound and attenuation measurements but our experience shows that averaging over a large number of scans at different lens positions X minimize their impact.

Subsequently, we recorded the corresponding shear Brillouin scattering data at the same X positions as for the longitudinal data by using the technique of enhanced generation and detection as described above. The shear speed of sound was then deduced from the phase shift extracted from depolarized scattering measurements. The fitting parameter in this case is the shear speed of sound. Like for the analysis of the longitudinal attenuation, the shear acoustic damping coefficient Γ_S was deduced from the measurement of the shear Brillouin amplitude

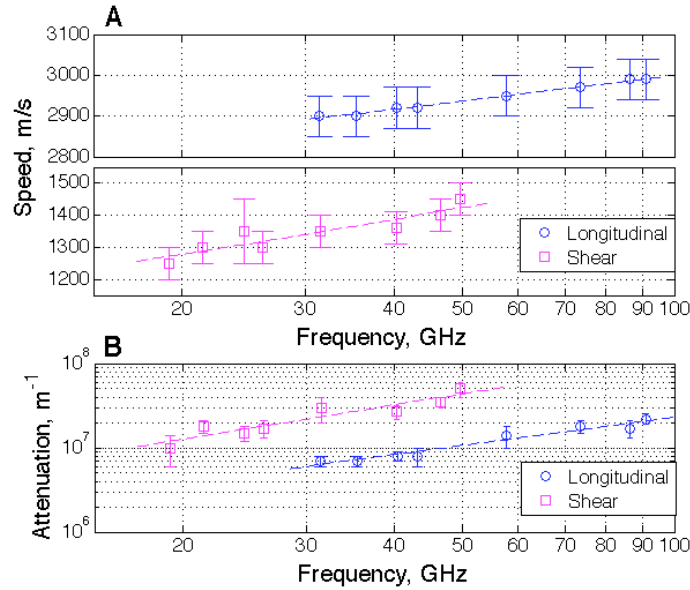


Figure 6.

Results of shear and longitudinal acoustic speeds (**A**) and attenuation coefficients (**B**) in liquid glycerol at room temperature.

by averaging over all calculated values of a data set at a given Brillouin frequency.

In order to obtain longitudinal and shear speed of sound and attenuation data over a broad range of Brillouin frequencies, we repeated our measurements for each tandem Brillouin frequencies by changing the probe refraction angle inside the substrate medium with the aid of a prism. In addition, we conducted experiments with either sapphire or glass as a gauge medium, which allowed us to access a longitudinal frequency range from 91 to 57 GHz with sapphire and 43 to 31 GHz with glass, and a shear frequency range from 50 to 31 GHz with sapphire and 26 to 19 GHz with glass. Figure 6 shows the results of the acoustic speed and attenuation measurements of glycerol.

Within the experimental uncertainties the shear and longitudinal speed of sound in liquid glycerol increases linearly with frequency which indicates a high elastic stiffening of the liquid at such high frequencies. The acoustic damping of both polarizations also increases linearly with the frequency and does not increase as ν^2 as commonly observed in solids or liquids^{29,30} and suggests that the shear viscosity η of the liquid becomes frequency dependent. The difference between liquids and solids refers to the dynamic viscosity which can be determined from the fundamental equation,²⁹ $\eta = \Gamma_S \rho v_S^3 / (2\pi\nu_S)^2 = 1.9$ mPa-s, with ρ being the density. This equation is valid when the acoustic wave vector $2\pi\nu/v_S$ exceeds the acoustic attenuation Γ_S ; in the present situation this is the case by a factor of 6, highlighting the viscoelastic propagation of the shear waves. Our calculated values for η are 1000 times smaller than the static viscosity of glycerol (close to the static viscosity of water³¹) indicating that the liquid to become less and less viscous at high frequency.

The measurements with water are slightly different than for glycerol. The reason is mainly because of the acoustic impedance mismatch between water and both surrounding solid media. The weakest detectable shear wave corresponds in this case to a liquid layer in the range of ten's of nanometers. As a consequence, it was not realistic to assume the liquid topography from the lens curvature. To overcome this problem, we used literature values for the longitudinal speed of sound in water. The liquid topography was then deduced from the analysis of the Brillouin longitudinal phase shift, assuming the value of the longitudinal speed of sound of $v_L = 1500$ ms⁻¹, taken from the reference.³² The analysis of the amplitude of the longitudinal Brillouin scattering enabled the determination of the longitudinal damping coefficient $\Gamma_L = 35 \cdot 10^6$ m⁻¹, slightly higher than for glycerol, see Fig. 6. From the shear depolarized Brillouin scattering measurements, conducted at similar lateral positions X,

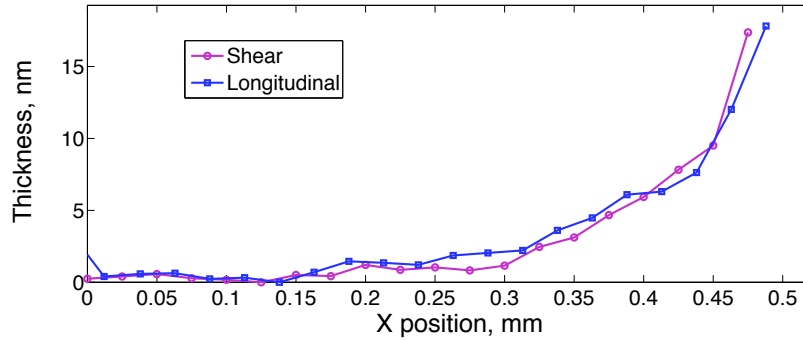


Figure 7.

Topography of a water layer at room temperature calculated from Brillouin scattering measurements at 42 GHz (longitudinal) and 25 GHz (shear).

with the advantage of the technique of enhanced Brillouin detection, we were able to detect a shear Brillouin frequency component at 25 GHz. This is contradictory with theoretical estimations claiming that "shear waves may be observed in liquids when the acoustic frequency exceeds the relaxation rate for viscous effects, estimated in the Maxwell rheological model for structural relaxation of water to be in the order of $\nu \sim 160 \text{ GHz}$ ".²⁷ Our experiment will help to better understand shear relaxation mechanisms in water. Moreover, by fitting the shear speed of sound that best match the longitudinal and the shear topography, see Fig. 7, we extracted the value of the shear speed of sound in water $v_S = 660 \text{ ms}^{-1}$. Subsequently, from the analysis of the shear Brillouin amplitude, we got a value for the attenuation $\Gamma_S = 120 \text{ } 10^6 \text{ m}^{-1}$, one order of magnitude higher than for glycerol at the same frequency. It is even possible to give a number concerning the viscosity of water at this frequency range. This is done, as previously, from the fundamental equation $\eta = \Gamma_S \rho v_S^3 / (2\pi\nu_S)^2 = 1.4 \text{ } 10^{-3} \text{ Pa}\cdot\text{s}$ and gives a value in really close agreement with the static value of $1 \text{ } 10^{-3} \text{ Pa}\cdot\text{s}$, telling that no shear relaxation peak is present at this frequency range. The ratio of the shear wavevector to the attenuation coefficient gives a value of $2\pi\nu_S / v_S \Gamma_S \sim 2 > 1$, telling that the shear wave at this frequency is purely viscoelastic rather than diffusive. This means that the shear threshold frequency of propagation is even lower.

Our measurement technique, an extension of conventional picosecond ultrasonics revealed new features of soft matter under ultrafast shear and longitudinal waves loading which cannot be accessed by other means. A full temperature-dependent study is under way to provide a deeper understanding of the underlying structural relaxation dynamics in glycerol and water. The frequency ranges that are accessible to the current method could be increased substantially by using 267 or 200 nm probe light (i.e. third or fourth harmonic of the 800 nm laser wavelength). It would be interesting to reach the threshold frequency for water, in order to detect the transition between the diffusive regime to the viscoelastic regime. Parallel efforts are under way to connect the frequency ranges of the present measurements with those of impulsive stimulated scattering measurements at MHz³³ to low GHz frequencies.

4. CONCLUSION

Recent progress on the generation and detection of picosecond shear acoustic waves in different media, as described in the present review, has reached the point where measurements of shear waves propagating in liquids have become possible. The key of this challenging problem have been the continuous effort on the improvement of shear photoacoustic transducers, with higher and higher efficiency at GHz frequencies. We believe that in the next decade, new kind of samples, still based on the principle of break-off shear symmetry, will reach THz frequencies for shear waves, as it is already the case for longitudinal waves. Finally, photoacoustic experiments might cover the frequency range from MHz to THz, at both longitudinal and shear polarizations.

ACKNOWLEDGMENTS

This work was partially supported by CNRS, the Department of Energy Grant No. DE-FG02-00ER15087 and National Science Foundation Grants No. CHE-0616939 and DMR-0414895. The authors would like to thank Vitaly Gusev for fruitful discussions and comments.

REFERENCES

- [1] C. Thomsen, J. Strait, Z. Varcling, H. J. Maris, J. Tauc, J. J. Hauser, Phys. Rev. Lett. **53**, 989 (1984).
- [2] H. T. Grahn, H. J. Maris, J. Tauc, IEEE J. Quantum Electron. **25**, 2562 (1989).
- [3] C. Thomsen, H. T. Grahn, H. J. Maris, J. Tauc, Phys. Rev. B **34**, 4129 (1986).
- [4] T. Pezeril, P. Ruello, S. Gougeon, N. Chigarev, D. Mounier, J.-M. Breteau, P. Picart V. Gusev, Phys. Rev. B **75**, 174307 (2007).
- [5] D. H. Hurley, O. B. Wright, O. Matsuda, V. E. Gusev and O. V. Kolosov, Ultrasonics **38**, 470 (2000).
- [6] O. Matsuda, O. B. Wright, D. H. Hurley, V. E. Gusev, K. Shimizu, Phys. Rev. Lett. **93**, 095501 (2004).
- [7] T. Pezeril, N. Chigarev, P. Ruello, S. Gougeon, D. Mounier, J.-M. Breteau, P. Picart, V. Gusev, Phys. Rev. B **73**, 132301 (2006).
- [8] T. Bienville and B. Perrin, Proc. WCU, 813 (2003), sfa.asso.fr/wcu2003/procs/website/.
- [9] T. Pezeril, F. Leon, D. Chateigner, S. Kooi, K. A. Nelson, Appl. Phys. Lett. **92**, 061908 (2008).
- [10] G. Tas, R. J. Stoner, H. J. Maris, G. W. Rubloft, G. S. Oehrlein, J. M. Halbout, Appl. Phys. Lett. **61**, 1787 (1992).
- [11] B. Bonello, F. A. Armand, J.-P. Pradeau, H. Perez, B. Perrin, G. Louis, J. Appl. Phys. **86**, 4959 (1999).
- [12] B. Bonello, G. Louis, P. Battioni, Rev. Sci. Instrument **74**, 889 (2003).
- [13] G. Tas, J. J. Loomis, H. J. Maris, A. A. Bailes, L. E. Seiberling, Appl. Phys. Lett. **72**, 2235 (1998).
- [14] G. A. Antonelli, B. Perrin, B. C. Daly, D. G. Cahill, MRS bulletin **31** n°8, 607 (2006).
- [15] H.-N. Lin, R. J. Stoner, H. J. Maris, J. M. E. Harper, C. Cabral, J. -M. Halbout, G. W. Rubloff, Appl. Phys. Lett. **61**, 2700 (1992).
- [16] *X-ray and neutron reflectivity*, J. Daillant and A. Gibaud, Springer, 87-115, (1999).
- [17] D. Chateigner,
www.ecole.ensicaen.fr/~chateign/texture/combined.pdf.
- [18] T. Pezeril, PhD Thesis, Université du Maine, tel.ccsd.cnrs.fr/tel-00011291 (2005).
- [19] T. Pezeril, V. Gusev, D. Mounier, N. Chigarev, P. Ruello, J. Phys. D : Appl. Phys. **38**, 1421 (2005).
- [20] P. Fréchar, S. Andrieu, D. Chateigner, M. Hallouis, P. Germe, M. Pernet, Thin Solid Films **263**, 42 (1995).
- [21] E. Donth, *The Glass Transition: : Relaxation Dynamics in Liquids and Disordered Materials*, Springer (2001).
- [22] Y. Yan, L. Cheng, K. A. Nelson, J. Chem. Phys. **88**, 6477 (1988).
- [23] S.M. Silence, A.R. Duggal, L. Dhar, and K.A. Nelson, J. Chem. Phys. **96**, 5448 (1992).
- [24] Y. Yang and K. A. Nelson, J. Chem. Phys. **103**, 7722 (1995).
- [25] Y. Yang and K. A. Nelson, J. Chem. Phys. **103**, 7732 (1995).
- [26] D. Paolucci, K. A. Nelson, J. Chem. Phys. **112**, 6725 (2000).
- [27] M. Msall, O. B. Wright, O. Matsuda, J. Phys. Conf. Ser. **92**, 4 (2007).
- [28] J. D. Choi, T. Feurer, M. Yamaguchi, B. Paxton, K.A. Nelson, Appl. Phys. Lett. **87**, 081907 (2005).
- [29] K. F. Herzfeld, T. A. Litovitz, *Absorption and Dispersion of Ultrasonic Waves*, Academic press, New York and London (1959).
- [30] C. J. Morath, H.J. Maris, Phys. Rev. B **54**, 203 (1996).
- [31] David R. Lide, *Handbook of Chemistry and Physics*, CRC Press (2007).
- [32] L. J. Shelton, F. Yang, W. K. Ford, and H. J. Maris, Physica Status Solidi B **242**(7), 13791382 (2005).
- [33] C. Glorieux, K. Van de Rostyne, J. Goossens, G. Shkerdin, W. Lauriks, K. A. Nelson, J. Appl. Phys. **99**, 013511 (2007).